Modification of Neutron Emission Spectra and Determination of Fuel Ion Ratio in Beam-Injected Deuterium–Tritium Plasma*)

Yasuko KAWAMOTO and Hideaki MATSUURA

Applied Quantum Physics and Nuclear Engineering, Kyushu University, 744 Motooka, Fukuoka 819-0395, Japan

(Received 1 December 2015 / Accepted 1 February 2016)

To stably control and operate a deuterium–tritium (DT) fusion reactor, it is important to accurately obtain the fuel ion ratio n_t/n_d (n is the number density). Previously, fuel ion ratio diagnostic methods using deuterium-deuterium (DD) and DT neutron emission rates have been studied. The reaction rate coefficients and neutron emission spectra, i.e., the shape and peak value, are strongly influenced by external plasma heating such as neutron beam injection (NBI) heating. In this paper, we consider the fuel ion ratio diagnostics by directly measuring the neutron emission spectra, including both beam–thermal and beam–beam fusion reactions, in deuterium beam-injected DT plasma. We also evaluate the slowing-down neutron component, i.e., noise, to examine whether the above method can be used for plasma diagnostics. On the basis of Boltzmann–Fokker–Planck and Monte Carlo neutron transport analyses, the applicability of the method to the beam-injected DT plasma is discussed. It is shown that the feasible plasma parameter regions of measuring for fuel ion ratio diagnostics is increased by beam injection and by adopting neutron detector channels shifted to the high-energy side.

Keywords: fuel ion ratio diagnostics, fusion blanket, neutron spectrometry, NBI, neutron transport simulation

DOI: 10.1585/pfr.11.2405078

1. Introduction

Neutron spectrometry plays an important role in deuterium-tritium (DT) fusion for plasma diagnostics, e.g., ion temperatures and fuel ion ratios. It is proposed that the fuel ion ratio, n_t/n_d, can be derived by measuring the intensity of neutron spectrum peaks by the deuterium–deuterium (DD) and DT reactions [1], i.e., $R_{DD} = (1/2)n_d^2 \langle\sigma v\rangle_{DD}$ and $R_{DT} = n_d n_t \langle\sigma v\rangle_{DT}$, where R is the reaction rate, n is the number density, and $\langle\sigma v\rangle$ is the reaction rate coefficient. The fuel ion ratio is obtained as

$$\frac{n_t}{n_d} = \frac{R_{DT}\langle\sigma v\rangle_{DD}}{2R_{DD}\langle\sigma v\rangle_{DT}}. \quad (1)$$

If the neutron emission spectrum conforms to a Gaussian function, the relationship between R and the measured peak value, N_{peak}, can be written as $N_{peak} = m_n R/4\pi^{3/2} v_n^0 \Delta$, where $\Delta \equiv (4m_n E_n^0 T/(m_{\alpha(\text{or } ^3\text{He})} + m_n))$ [2]. Here E_n^0 is the neutron emission energy at the center of mass system, v_n^0 is the corresponding velocity, and T denotes the ion temperature. A problem that complicates this measurement has been pointed out in a previous study [3, 4]. Because the DT reaction rates are significantly higher than that of the DD reactions during a normal operation in a DT fusion reactor, the deceleration of neutrons in the structural materials caused by the DT reaction are detected as noise for DD signals.

So far, the neutron spectrum for ITER was evaluated under various conditions, and it has been shown that neutron emission spectroscopy meets the requirements for $n_t/n_d < 0.6$ [5]. To realize this method in future fusion reactors, further improvements in the neutron signal are required.

Generally, the following methods are used to improve the signal of DD neutrons under various conditions:

- Reducing a noise by setting up a collimator for the measurement instrument.
- Increasing the DD reaction rate using the Neutron Beam Injection (NBI) [5].

Hellesen *et al.* proposed a fuel ion ratio diagnostic method using the ratio of thermonuclear emission to beam-target neutron emission in the beam-injected DT plasma [6, 7]. The method was applied to NBI-heated DT plasmas at JET. Even though some discrepancies in the results obtained by other methods have been reported for fuel ion ration measurements in the core region, this method is one of the most promising.

In beam-injected plasmas, depending on the plasma heating conditions, not only the reaction rate coefficient but also the shape of the neutron emission spectra significantly changed. DT noise could be relatively reduced compared with DD signals if the degree of enhancement for the DD reaction rate coefficient was much larger than that for DT. However, in this case, it should be noted that the shape of the neutron emission spectra of both the DD and DT neutrons are also changed. This implies that the values of the

author's e-mail: kawamoto@nucl.kyushu-u.ac.jp

*) This article is based on the presentation at the 25th International Toki Conference (ITC25).

neutron peaks with and without beam injection are different. These values depend on the plasma or the NBI conditions, and accurate simulations of the velocity distribution functions and neutron emission spectra are necessary.

In this paper, we consider the fuel ion ratio diagnostics by directly measuring the neutron emission spectra, including both the beam–thermal and beam–beam fusion reactions in the deuterium beam-injected DT plasma. Our goal is to demonstrate the improvement in the fuel ion ratio diagnostic accuracy by using NBI. The simulation is based on the Boltzmann–Fokker–Planck (BFP) model [8] and the Monte Carlo neutron transport simulation. We evaluated the DT neutron noise for an ITER shielding blanket to examine whether the above method can be used for plasma diagnostics. The applicability of the method to beam-injected DT plasma is then discussed.

2. Analysis Model

2.1 Boltzmann–Fokker–Planck model

In this study, we use the BFP model. The ion distribution function with/without NBI can be found by simultaneously solving the following BFP equations for ion species i (i = d, t, α, proton, and ^{3}He):

$$\sum_j \left(\frac{\partial f_i}{\partial t}\right)_j^{\mathrm{C}} + \sum_k \left(\frac{\partial f_i}{\partial t}\right)_k^{\mathrm{NES}} + \frac{1}{v_i^2}\frac{\partial}{\partial v_i}\left(\frac{v_i^3 f_i}{2\tau_{\mathrm{C}}^{i*}(v_i)}\right) + S_i(v_i) - L_i(v_i) = 0, \quad (2)$$

where $f_i(v_i)$ is the distribution function for the species i. The first term in Eq. (2) represents the coulomb collision and j indicates particles in the background, e.g., d, t, α, proton, ^{3}He, and electron. The second term represents the effect of nuclear elastic scattering (NES) [9], and k indicates the background ions, e.g., d, t, α, proton, and ^{3}He. We consider the NES scattering between the following: 1) α and D, 2) α and T, 3) α, and ^{3}He, 4) proton and D, 5) proton and T and 6) proton and ^{3}He, i.e., (i, k) = (D, α), (T, α), (^{3}He, α), (α, D), (α, T), (α, ^{3}He), (D, p), (T, p), (^{3}He, p), (p, D), (p, T) and (p, ^{3}He). The cross-sections for NES are taken from the work of Perkins and Cullen [10]. Energy loss due to thermal diffusion is considered in the third term. To incorporate the unknown loss mechanism of energetic ions into the analysis, we simulated the velocity-dependence of the energy loss due to thermal conduction $\tau_{\mathrm{c}}^{i*}(v)$ and particle-loss time $\tau_{\mathrm{p}}^{*}(v)$ using a dimensionless parameter γ [11], i.e.,

$$\tau_{\mathrm{c(p)}}^{i*}(v) = \begin{cases} C_{\mathrm{c(P)}}^{i}\tau_{\mathrm{c(P)}}^{i} & \text{when } v < v_{\mathrm{th}}^{i} \\ C_{\mathrm{c(P)}}^{i}\tau_{\mathrm{c(P)}}^{i}(v/v_{\mathrm{th}})^{\gamma} & \text{when } v \geq v_{\mathrm{th}}^{i}, \end{cases} \quad (3)$$

where v_{th}^{i} is the thermal velocity of the ion species i. The source ($S_i(v)$) and loss ($L_i(v)$) terms take a different form for each ion species [12].

The neutron emission spectrum can be computed by applying the distribution function determined using the BFP equations to the following equation:

$$\frac{\mathrm{d}N_{\mathrm{n}}}{\mathrm{d}E}(E) = \iiint f_{\mathrm{D}}(|\vec{v}_{\mathrm{D}}|) f_{\mathrm{T(D)}}(|\vec{v}_{\mathrm{T(D)}}|) \frac{\mathrm{d}\sigma}{\mathrm{d}\Omega} \times \delta(E - E_{\mathrm{n}})\vec{v}_{\mathrm{r}}\mathrm{d}v_{\mathrm{D}}\mathrm{d}v_{\mathrm{T(D)}}\mathrm{d}\Omega, \quad (4)$$

E_{n} is given [13] by

$$E_{\mathrm{n}} = \frac{1}{2}m_{\mathrm{n}}V_{\mathrm{c}}^2 + \frac{m_{\alpha(^3\mathrm{He})}}{m_{\alpha(^3\mathrm{He})} + m_{\mathrm{n}}}(Q_{\mathrm{DT(DD)}} + E_{\mathrm{r}}) + V_{\mathrm{c}}\cos\theta_{\mathrm{c}}\sqrt{\frac{2m_{\alpha(^3\mathrm{He})}m_{\mathrm{n}}}{m_{\alpha(^3\mathrm{He})} + m_{\mathrm{n}}}(Q_{\mathrm{DT(DD)}} + E_{\mathrm{r}})}, \quad (5)$$

where N_{n} is the neutron emission rate and $\mathrm{d}\sigma/\mathrm{d}\Omega$ is the differential cross section for the DT reaction. Equation (5) represents the kinetic energy of the neutron in the laboratory system. Therefore, V_{C} is the center of mass velocity between the deuteron and triton, E_{r} is the relative energy of the deuteron and triton in the laboratory system, $Q_{\mathrm{DT(DD)}}$ is the reaction Q-value for the DT (DD) reaction, i.e., 17.59 (3.27) MeV, and θ_{C} is the angle between the center of mass velocity and velocity of the emission particle. For these the calculations, the cross sections of fusion reactions were taken from the work of Bosch [14].

2.2 Neutron transport simulation

In this study, the simulation to obtain the neutron spectra at ITER [15] was conducted using the Monte Carlo transport code MVP [16] with the JENDL3-3 [17] nuclear data library. The calculation model was employed the torus form (Fig. 1), which has a 6200 mm major radius and a 2600 mm minor radius (Table 1). The neutron source was assumed to be generated isotropically at the line along the magnetic axis. We assumed a uniform blanket in both the poloidal and toroidal directions. Therefore, the difference in the neutron flux between the wall positions was entirely caused by the geometric shape of the confinement device. We can reduce the difference by using a collimator because the difference is caused by incident neutrons with large angles to the wall. Therefore, the discussion in this paper does not depend on the position of the collimator, and the neutrons can be measured using a collimator placed between the plasma and the blanket in the equatorial plane of the outboard side. We simulated the detector using the calculation model, which has a detection surface (Fig. 2). The

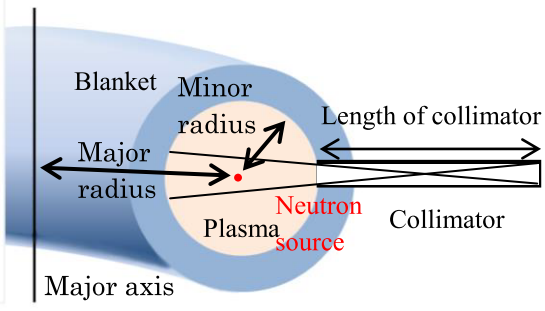

Fig. 1 Calculation model.

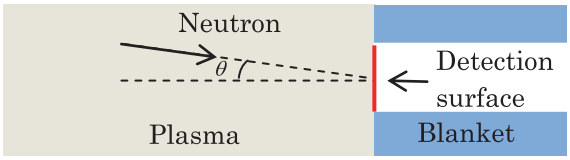

Fig. 2 Detector model.

Table 1 Shape of the reactor.

	(mm)
Major radius	6200
Minor radius	2600
Collimator radius	30
Length of the collimator	$2\times30/\tan\theta$

Table 2 Shape and components of the blanket.

	Thickness (mm)	Composition (%)
Be armor	10	Be(100)
CuCrZr heat sink	22	CuCrZr(82.9), H_2O(17.1)
First Wall structure	49	SS316L(N)-IG(84.6), H_2O(15.4)
Gap	3	
Shield structure	370	SS316L(N)-IG(72), H_2O(18)

detectable incident angle of the neutron, θ, was restricted to correspond to the change in the length of the collimator. The shape and component design parameter of the blanket is shown in Table 2 [15]. We assumed a uniform material composition for each blanket layer.

3. Results and Discussion

In this study, the energy resolution of the neutron spectrometer was set to 280 keV in accordance with the target value of ITER (2 % for 14 MeV) [18]. Throughout the simulation, the electron temperature, T_e = 10 keV , energy confinement time, τ_E = 2.8 sec, beam injection energy, E_{NBI} = 1.0 MeV, and the maximum incident angle of the detectable neutron, θ = 5°, were assumed.

The deuteron distribution derived from the BFP model is shown in Fig. 3. The tail was formed around the 1.0 MeV energy range because the beam injection energy was 1.0 MeV. As the electron density decreased, the relative intensity of the energetic non-Maxwellian component increases. This occurred because the slowing-down effect was weakened by the reduced background density. Therefore, the neutron emission spectra in the low-density plasma obtained by Eqs. (4) and (5) using the ion distribution with large distortion significantly departed from a Gaussian (Figs. 4 and 5). In such a case, the reaction rate coefficients of both the DD and DT reactions were also enhanced. The modification of the neutron emission spectra becomes larger on the high-energy side compared with the low-energy side. This is an important factor to increase S/N (S represents the source, which is the neutron spectrum generated by the DD reaction, and N represents the noise, which is the neutron spectrum generated by the DT

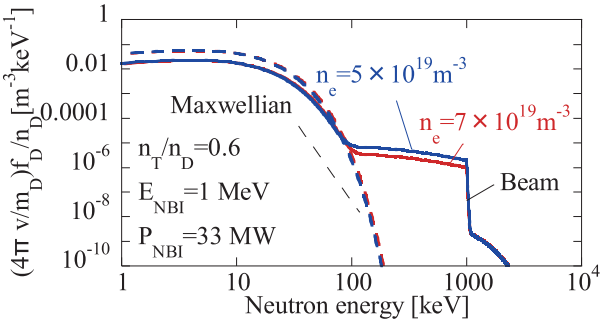

Fig. 3 Deuteron distribution functions.

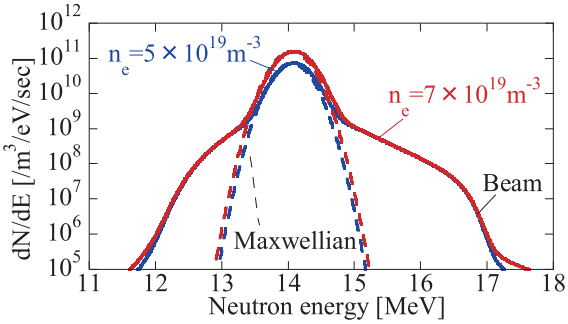

Fig. 4 Neutron spectra for the DT reaction.

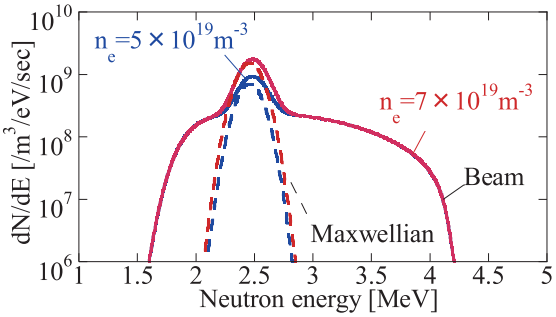

Fig. 5 Neutron spectra for the DD reaction.

reaction in the energy measuring range). To increase S/N implies to improve the performance of the measurement. Therefore, we prepared two patterns of the energy range for the S/N measurement, e.g., 2.18 - 2.74 MeV (channel A) and 2.32 - 2.88 MeV (channel B).

We estimated the feasibility of the fuel ion ratio measurement by comparing the obtained S/N values for various electron densities with the standard value when n_t/n_d = 0.6 and channel A were assumed. Ericsson, *et al.* have pointed out that fuel ion ratio diagnostics using the DD and DT neutron spectra are available under the condition that n_t/n_d < 0.6 and T > 6 keV [5]. Figure 6 shows the S/N values when n_t/n_d = 0.6 and 1.0 for various electron densities. It was found that the S/N values (channel A without beam injection) tend to decrease with increasing n_t/n_d ratios. This is because the ratio of the DD to DT reactions rate was reduced by the increased triton density. Therefore, when

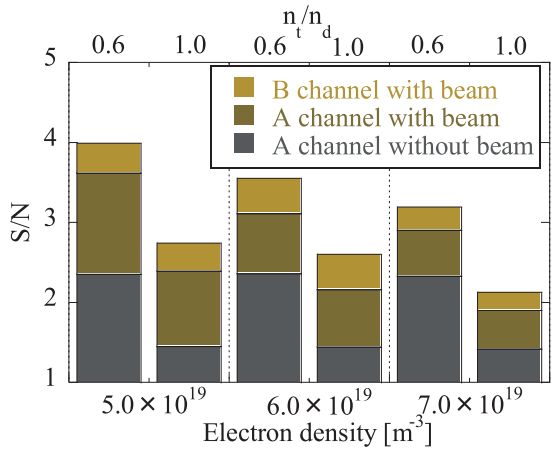

Fig. 6 S/N values for various electron densities.

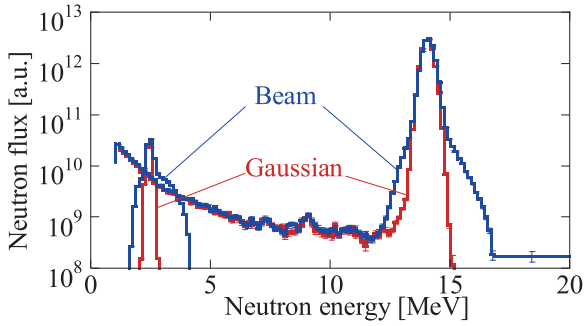

Fig. 7 DD and DT neutron fluxes when upon deuterium beam injected.

$n_t/n_d = 1.0$ (channel A without beam injection), it is difficult to use the present diagnostic method, as was pointed out by Ericsson *et al.*, i.e., the S/N values are lower when $n_t/n_d = 1.0$ than those when $n_t/n_d = 0.6$.

We observed that the S/N values increase by using beam injection and by adopting channel B. The S/N value improves with beam injection because the enhancement in the DD reactivity due to the non-Maxwellian tail formation is larger than that in the DT reaction. Even though the peak value of the neutron spectrum tends to decrease because of the modification of the spectrum due to beam injection, the effect of the DD reactivity enhancement is more influential than the effect of the spectrum peak reduction. We also observed that the S/N values are further increased when channel B is adopted. This is because that the spectra are extended to the higher-energy side rather than the lower-energy side as a result of beam injection (Fig. 7). By choosing a higher energy range as the focused channel, the DT noise decreases and S/N value is improved. As indicated in Fig. 6, the spectrum modification effect weakens at high-density range. This is because the slowing-down effect for energetic ions is enhanced by the increased collision rate in high-density plasma, i.e., the non-Maxwellian tail becomes small. As shown in Fig. 6, by adopting beam injection, similar S/N values when $n_t/n_d = 0.6$ without NBI are obtained when $n_t/n_d = 1.0$. This implies that the diagnostics using the present method become accessible in the $n_t/n_d = 1.0$ range when NBI is adopted. When $n_e = 7 \times 10^{19}$ m^{-3}, the S/N value for the beam-injected operation is slightly smaller than that when $n_t/n_d = 0.6$ without NBI. However, by increasing the beam injection power from 33 to 50 MW [19], the S/N value reaches approximately 2.3; therefore, the fuel ion ratio diagnostic using the DD and DT spectra becomes accessible when $n_t/n_d = 1.0$ and $n_e = 7 \times 10^{19}$ m^{-3}.

4. Conclusion

On the basis of the Boltzmann–Fokker–Planck and Monte Carlo neutron transport analyses, the applicability of the fuel ion ratio diagnostic method in a DT plasma is examined. It is shown that the feasible plasma parameter regions of measuring for fuel ion ratio diagnostic is increased with beam injection and by adopting a neutron detector energy channel shifted to the high-energy side.

[1] J. Källne *et al.*, Rev. Sci. Instrum. **62**, 2871 (1991).
[2] G. Lehner and F. Pohl, Zeitschrift für Physik **207**, 83 (1967).
[3] F. Moro *et al.*, Fusion Eng. Des. **86**, 1277 (2011).
[4] V.G. Kiptily, Nucl. Fusion **55**, 023008 (2015).
[5] G. Ericsson *et al.*, Rev. Sci. Instrum. **81**, 10D324 (2010).
[6] C. Hellesen *et al.*, Rev. Sci. Instrum. **83**, 10D916 (2012).
[7] C. Hellesen *et al.*, Nucl. Fusion **55**, 023005 (2015).
[8] H. Matsuura *et al.*, Phys. Plasma **13**, 062507 (2006).
[9] J.J. Devaney *et al.*, Nucl. Sci. Rng. **46**, 323 (1971).
[10] S.T. Perkins *et al.*, Nucl. Sci. Eng. **20**, 77 (1981).
[11] E. Bittoni *et al.*, Nucl. Fusion **29**, 931 (1980).
[12] H. Matsuura *et al.*, Plasma Phys. Control. Fusion **53**, 035023 (2011).
[13] H. Brysk, Plasma Phys. **15**, 611 (1973).
[14] H.S. Bosch and G.M. Hale, Nucl. Fusion **32**, 611 (1992).
[15] M.E. Swan *et al.*, Proceedings of the 22nd IEEE / NPSSS symposium on Fusion Engineering, Albuquerque, NM, June 17-21, 1 (2007).
[16] Y. Nagaya *et al.*, JAERI 1348 (2005).
[17] K. Shibata *el al.*, J. Nucl. Sci. Technol. **39**, 1125 (2002).
[18] T. Nishitani *et al.*, J. Plasma Fusion Res. **80**, 860 (2004) (in Japanese).
[19] R. Hemsworth *et al.*, Nucl. Fusion **49**, 045006 (2009).